Structural Chemistry (2019) 30:1843–1852
https://doi.org/10.1007/s11224-019-01294-0

ORIGINAL RESEARCH

Water-gas-shift reaction over nickel catalysts: DFT studies and kinetic modeling

Ali Nakhaei Pour[1] · Sayyed Faramarz Tayyari[1]

Received: 6 October 2018 / Accepted: 21 January 2019 / Published online: 22 March 2019

Abstract
Density functional theory (DFT) calculations were used to study the mechanism of water gas shift (WGS) reaction on Ni (111) surfaces. Three sets of elementary reactions based on the formate intermediate and oxidation-reduction mechanisms are considered in this study. Formate intermediate is produced via dissociation and non-dissociation adsorption of H_2O in the proposed mechanisms. The adsorption energy for all surface species and the activation barriers for the rate-determining steps in these WGS mechanisms were calculated. The overall reaction rates were developed based on the considered mechanisms. Based on the Sabatier principle, the effects of CO and H_2O adsorption energies on the activation energy of the rate-determining reactions in the proposed mechanisms are considered. According to the calculated overall activation energies, the formate intermediates produced from the reaction between adsorbed H_2O and CO species provide the best condition for the overall WGS reaction.

Keywords Water gas shift reaction · DFT · Micro-kinetic · Nickel · Catalyst

Introduction

The world's development towards the hydrogen economy in fuel cells and oil refining is facilitating the production of hydrogen from various resources [1]. The water-gas-shift (WGS) reaction is a key step in the generation of hydrogen from carbon-based materials in industrial plants [2]:

$$CO + H_2O \rightleftharpoons CO_2 + H_2 \qquad \Delta H_{298K} = -41\ \text{kJ mol}^{-1} \quad (1)$$

The reaction is catalyzed by a number of different base metal catalysts, depending on the operating temperature and levels of poisons in the feedstock. Wheeler et al. studied the possibility of the WGSR using noble metals in the temperature range of 550 to 1300 K and found the activity of the metals in the order, Ni > Ru > Rh > Pt > Pd [3]. Nickel-based catalysts are promising single-stage WGS catalysts, but the surface reaction mechanism on this type of catalysts was not well understood [4].

✉ Ali Nakhaei Pour
a.nakhaei@um.ac.ir; nakhaeipoura@yahoo.com

[1] Department of Chemistry, Faculty of Science, Ferdowsi University of Mashhad, Mashhad 91775-1436, Iran

In situ spectroscopy results show the presence of formate, carboxyl, and carbonate intermediates over Ni surfaces [5, 6]. Two overall mechanisms have been proposed for the WGS reaction over metal catalysts: formate and direct oxidation [7–9]. Indirect oxidation mechanism, it is assumed that the adsorbed CO species are oxidized to CO_2 and reduces the oxidized site to complete the cycle [10]. In the formate mechanism, it is assumed that the formate, carboxyl, and or carbonate intermediates are formed on the surface of catalysts through the reaction between carbon monoxide and a hydroxyl species or water. These intermediates decompose to hydrogen and carbon dioxide [7]. Catapan et al. report the results of a systematic density functional theory (DFT) study of the WGS reaction and coke formation pathways on Ni (111) and Ni (211) surfaces [4]. They suggested that the WGS reaction occurs mainly via the formate mechanism and carboxyl pathway as the rate-determining step. Mohsenzadeh et al. used the DFT calculations to study the WGS reaction on Ni (111), Ni (100), and Ni (110) surfaces [11]. Their results show that the WGS reaction does not primarily occur via the formate pathway. Lin et al. used DFT calculations to investigate the WGS reaction on a series of transition metals including the Ni (111) surface [12].

The kinetic modeling of the WGS reaction on iron catalysts was investigated in our previous works [8, 9, 13]. These results show that the WGS rate expressions based on the formate mechanism provide an improved description for WGS

reaction. In the present work, a systematic DFT study of the WGS reaction on Ni (111) surface based on the most important reaction pathways was performed.

Computational and theoretical methods

DFT calculations

The density functional theory (DFT) model calculations were consisted on (111) surface of nickel face-centered cubic (FCC) metallic phase (111) within the three-metal-layer slab model approximation. Semi-infinite nickel crystal surfaces with a p(2 × 2)unit cell were used to model the 1/4 and 1/2 monolayer (ML) coverage for one or two adsorbates, respectively. The relative positions of the metallic atoms were initially fixed at their original positions in the bulk, and the optimized lattice parameter was selected as 3.524 Å [14].

All quantum chemical *calculations were* carried out with Quantum ESPRESSO program package, which performs an iterative solution of Kohn–Sham equations in a double-zeta plus polarization (DZ) basis set [15, 16]. The localization radii of the basis functions were determined from an energy shift of 0.01 eV [17]. A standard DFT supercell approach with the revPBE-D_3(BJ) form of the generalized gradient approximation (GGA-D) functional was used, and the Kohn–Sham orbitals were expanded in a localized basis (double-zeta). Spin polarization was included in the calculations. Fermi smearing with an s = 0.2 eV was used to account for fractional occupancies. All optimized geometries corresponded to the minimum or transition states (TSs) were checked by the normal mode vibrational analysis. Only the adsorbates were allowed to move on the surface, and all Ni atoms are fixed at their observed face-centered cubic positions [18]. The vibration frequency calculations confirmed that the stationary structures were in the minimum energy geometries (no imaginary frequencies) or transition states (one imaginary frequency).

The adsorption energy of the adsorbate is given by

$$E_{ads} = E_{adsorbate/slab} - E_{adsorbate} - E_{slab} \quad (2)$$

where $E_{adsorbate/slab}$ is the total energy of the surface of the slab with the adsorbate which is adsorbed on the surface, $E_{adsorbate}$ is the total energy of the isolated adsorbate, and E_{slab} is the total energy of the surface of slab without of adsorbate.

Micro-kinetic model

The formate and its direct oxidation mechanisms have been proposed for the WGS reaction over metal catalysts [7]. Indirect oxidation mechanism assumes that the H_2O molecules adsorb and dissociates on suitable surface sites to produce hydrogen and oxidizing the site. Then, the adsorbed carbon monoxide is oxidized to CO_2 and reduces the oxidized site to complete the oxidation-reduction cycle. In formate mechanism, formate, carboxyl, and/or carbonate intermediates are formed through the reaction between carbon monoxide and an adsorbed hydroxyl species or water, which then decomposes to hydrogen and carbon dioxide molecules. The adsorbed hydroxyl species is formed via decomposition of adsorbed water molecules [7, 8, 12].

Three sets of elementary reactions based on the formate intermediate (WGS I, WGS II) and direct oxidation mechanism (WGS III) for the WGS reaction are considered in our previous work and listed in Table 1 [9]. In the WGS I model, it is assumed that the formate intermediate is produced from the reaction between adsorbed water and carbon monoxide molecules. In the second model (WGS II), it is assumed that H_2O is dissociatively adsorbed; the formate intermediate is produced from the reaction between OH and CO surface species. Model WGS III is based on the oxidation-reduction mechanism and assumes that the H_2O molecule adsorbs dissociatively on the surface.

The rate constant (k) for forward (k_f) and reverse (k_b) of each elementary reaction was estimated from transition state theory using Eq. (3) [19]:

$$k = \left(\frac{k_B T}{h}\right)\left(\frac{q^{\neq}}{q}\right)\exp\left(\frac{-E_a}{k_B T}\right) \quad (3)$$

where E_a is the activation energy, k_B is Boltzmann's constant, h is Planck's constant, and T is the absolute temperature. Also,

Table 1 Elementary reaction steps for WGS reaction

Model	Reaction step	Elementary reactions
WGS I	S1	$CO + s \rightleftharpoons COs$
	S2	$H_2O + s \rightleftharpoons H_2Os$
	S3	$COs + H_2Os \rightleftharpoons COOHs + Hs$
	S4	$COOHs + s \rightleftharpoons Hs + CO_2s$
	S5	$CO_2s \rightleftharpoons CO_2 + s$
	S6	$2Hs \rightleftharpoons H_2 + 2\ s$
WGS II	S1	$CO + s \rightleftharpoons COs$
	S2	$H_2O + s \rightleftharpoons H_2Os$
	S3	$H_2Os + s \rightleftharpoons OHs + Hs$
	S4	$COs + OHs \leftrightarrow COOHs + s$
	S5	$COOHs + s \rightleftharpoons Hs + CO_2s$
	S6	$CO_2s \rightleftharpoons CO_2s + s$
	S7	$2Hs \rightleftharpoons H_2 + 2\ s$
WGS II	S1	$CO + s \rightleftharpoons COs$
	S2	$H_2O + 2s \rightleftharpoons OHs + Hs$
	S3	$OHs + s \rightleftharpoons Os + Hs$
	S4	$COs + Os \rightleftharpoons CO_2s + s$
	S5	$CO_2s \rightleftharpoons CO_2 + s$
	S6	$2Hs \rightleftharpoons H_2 + 2\ s$

in Eq. (3), q and $q^{\#}$ are the partition functions for the reactant and the transition state, respectively, which are estimated from assuming harmonic vibrations. Based on the calculated k_f and k_b, the equilibrium constant K_{eq} is obtained by the following equation:

$$K_{eq} = \frac{k_f}{k_b} \tag{4}$$

Results and discussion

Dissociation mechanism of H_2O

The kinetically important step in WGS reaction is the adsorption and decomposition of H_2O [11, 20]. As mentioned above, in the reaction of water gas shift, the first step of reaction sequence is the decomposition of H_2O into OH species and hydrogen. The adsorption energies of these various surface species play an important role in the H_2O dissociation on the surface of the nickel catalyst. The adsorption energies, adsorption sites, distance between oxygen and hydrogen atoms and nickel atoms are provided in Table 2. The geometry of adsorbed H_2O, OH, and H species is shown in Fig. 1.

As shown in Table 2, the adsorption energy of H_2O is − 0.24 eV for the top site of Ni (111) surface, which is in very good agreement with the reported values [4, 11]. The distance between the oxygen atom and the nearest Ni atom is 2.226 Å, and the two O–H bonds have the same lengths on the Ni (111) surface (0.987 Å) and H–O–H angle is 104.8° (Table 2). The O–H bond lengths and H–O–H angle for the isolated water molecule are 0.973 Å and 104.2°, respectively, which are smaller than the adsorbed water on Ni (111) surface.

Mohsenzadeh et al. calculated the H_2O adsorption energies of − 0.26 eV, oxygen-nickel distances of 2.225 Å and O–H bond lengths of 0.982 for Ni (111) surface [20]. Fajín et al. reported water adsorption energies of − 0.32 eV, surface-adsorbate distances of 2.23 Å, and O–H bond lengths of 0.98 Å for Ni (111) surface [21]. Seenivasan et al. obtained the H_2O adsorption energies of − 0.17 eV,= and O–H bond lengths of 0.98 Å for Ni (111) surface [22].

As shown in Table 2, the adsorption energies, O–Ni bond length for OH adsorbs on the nickel top site, and O–H bond length for top OH species are calculated about − 3.44 eV, 1.974 Å, and 0.976 Å. Zhou et al. calculated adsorption energy of − 3.37 eV with a Ni–O distance of 2.09 Å for OH adsorption on the Ni (100) surface [40]. Seenivasan et al. reported the adsorption energies of − 3.31 and − 3.57 eV, and O–H bond lengths of 0.97 and 0.98 Å for OH adsorbed on the Ni (111) and Ni (100) surfaces, respectively [23]. In addition, O species adsorbs on the bridge site and adsorption energy and bonding distance of O–Ni is − 5.45 eV and 1.852 Å, respectively. Finally, H atom adsorbs on the top site of nickel atoms with the adsorption energy of − 2.87 eV and the bonding distance of H–Ni is 1.756 Å, which is well consistent with reported values [11, 20]. Christmann et al. used experimental methods of low energy electron diffraction (LEED) and thermal desorption spectroscopy (TDS) to study the adsorption of hydrogen atoms on the Ni (111) surface [24]. They observed that H atoms located on the threefold hollow site with a Ni–H bond length of 1.84 Å.

Table 2 Adsorption energies and structural parameters of adsorbed species

Species	E_{ads} (eV)	$d_{surf\text{-}ads}$ (Å)	Bond length (Å)	Bond angle (°)
H_2O	− 0.24	2.226	O–H, 0.987	$\theta_{H\text{-}O\text{-}H}$, 104.8
OH	− 3.44	1.974	O–H, 0.976	–
H	− 2.87	1.756	–	–
O	− 5.45	1.852	–	–
CO_2	− 0.04	3.843	C–O, 1.16	$\theta_{O\text{-}C\text{-}O}$, 180
CO	− 1.68	2.21	C–O, 1.12	–
COOH	− 2.72	2.12	C–O, 1.17	–
H_2	− 1.19	1.937	H–H, 0.758	–

Adsorption of other surface species

The experimental results of CO_2 adsorption on nickel catalysts indicate that CO_2 binds in the physisorption regime (< 10 kcal/mol). In this work, the CO_2 adsorption on Ni (111) surface is considered as a physisorption process, with the adsorption energy equal to − 0.04 eV and C–Ni bond length equal to 3.843 Å for top sites, which is well consistent with previous results [11, 20, 25]. These adsorbed CO_2 molecules are produced from surface CO, COOH, and O species in formate and direct oxidation mechanisms. The adsorption energies of these various surface species play an important role in the CO_2 formation on the surface of nickel catalysts. The adsorption energies, adsorption sites, distance between surface species, and nickel atoms are presented in Table 2.

The carbon monoxide molecule binds to the surface via its carbon atom on the top site with the C–Ni binding energy and bonding distance of − 1.68 eV and 2.21 Å, respectively, which is in good agreement with the reported values [11, 20, 26] and experimental calorimetric results by Stuckless et al. [27]. Calculated heats of adsorption in this work are about 0.4 eV higher than the experimental values. This difference may be related to the zero-surface occupation and slab structure in our calculation, which cannot accurately predict CO binding energy. For COOH, the binding energy and bonding distance of C–Ni are − 2.72 eV and 2.12 Å, respectively, on the top site Ni (111) surface. The formate intermediate binds strongest to the Ni (111) surface; both oxygen atoms are adsorbed on the top sites with similar distances.

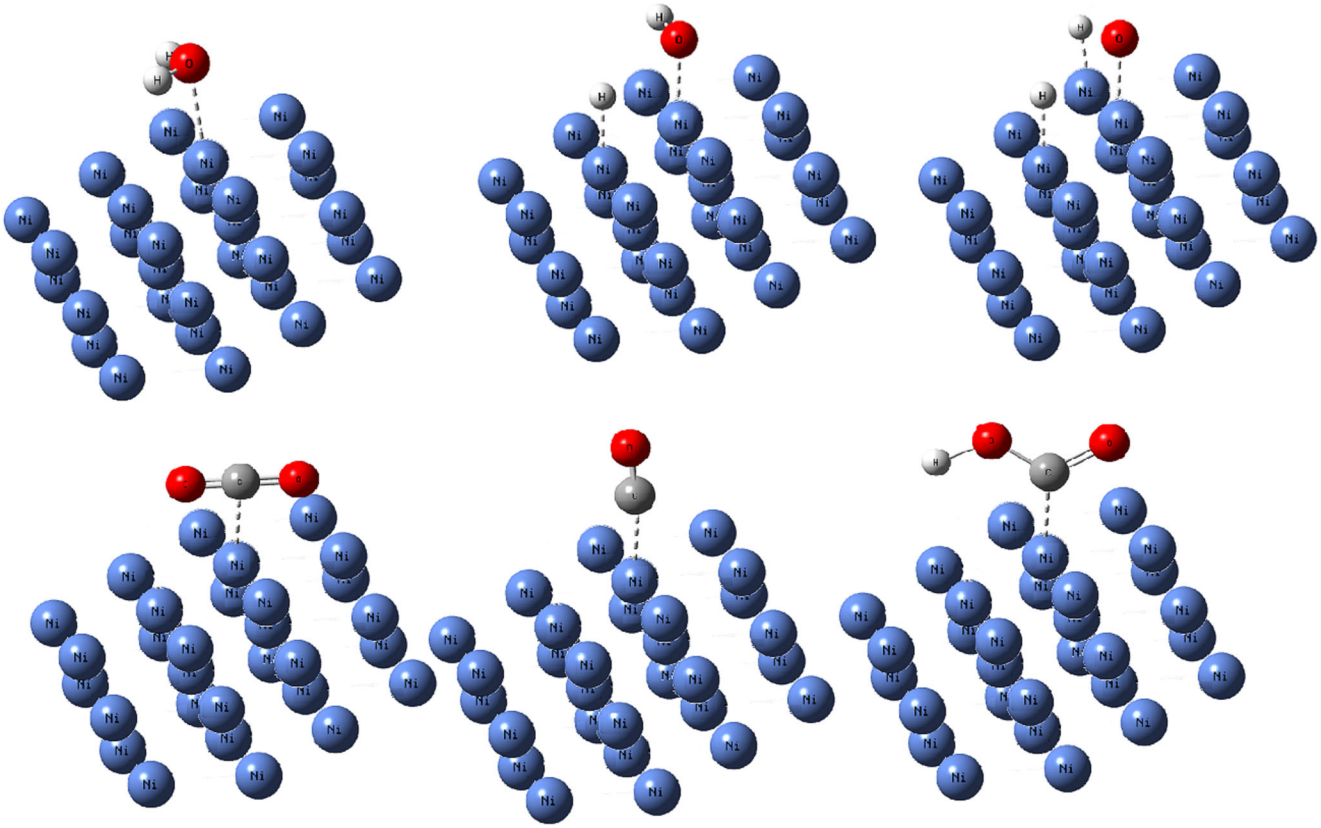

Fig. 1 The geometry of adsorbed H_2O, OH, O, CO_2, CO, COOH, and H species

The H_2 molecule binds to the top site of Ni (111) surface. The binding energy of H_2 is calculated as follows:

$$E_{ads\ of\ \ H2} = 2E_{H/slab} - [E_{H2} + 2E_{slab}] \quad (5)$$

where $E_{H/slab}$ is the total energy of the slab with the chemisorbed atomic H on the surface, E_{H2} is the energy of the H_2 molecule, and E_{slab} is the energy of the slab. Using Eq. (3), we obtain the adsorption energies of − 1.19 with 1.937 Å Ni–H distance, for hydrogen on the Ni (111) surface. These results are also in good agreement with previously reported experimental data [28].

Reaction activation energies

The activation energies of forward ($E_{a.f}$) and reverse reactions ($E_{a.b}$), the forward reaction rate constant (k_f), the reverse reaction rate constant (k_b), and the equilibrium constant (K_{eq}) for essential elementary reactions of WGS I, WGS II, and WGS III mechanisms are summarized in Table 3. As shown in this table, in the WGSI mechanism, the adsorbed H_2O react directly with the adsorbed carbon monoxide. However, in the WGSII mechanism, the reaction starts by H_2O dissociation to OH and H on the surface of the catalyst, while the adsorbed carbon monoxide reacts directly with the adsorbed OH. In WGS III mechanism, carbon monoxide can react with the water dissociation product (O) via the direct oxidation pathway. As shown in Table 3 for WGSII mechanism, the water dissociation barriers are larger than the adsorption energies for water on the Ni (111) surface. Therefore, it is expected that most of the water molecules desorbed without proceeding to OH and H species like that considered in WGS I mechanism.

In WGS I mechanism, the adsorbed carbon monoxide reacts with the adsorbed H_2O molecule to form COOH on the surface. This adsorbed COOH is bonded to the surface via its carbon atom. The calculated activation energy for this step is 1.93 eV on the Ni (111) surface. In the fourth step of the WGS I mechanism, the formate intermediate (COOHs, Table 3) subsequently dissociates to adsorbed carbon dioxide and adsorbed hydrogen with an activation energy of 0.63 eV. The detailed configurations of initial, transition, and final states involved in WGS I (S_4 reaction step) and WGS II (S_4 reaction step) mechanisms are shown in Fig. 2. As shown in Fig. 2, the C–O bond length and O–C–O bond angle changed from 1.19 Å and 163.1° in the transition state to 1.16 Å and 179.9° in adsorbed carbon dioxide, respectively.

The third step of water gas shift reaction in WGSII mechanism is the dissociation of adsorbed water molecules. As

Table 3 Activation barriers of forward reaction ($E_{a,f}$) and reverse reaction ($E_{a,b}$), forward reaction rate constant (k_f), reverse reaction rate constant (k_b), and equilibrium constant (K_{eq}) for important elementary reactions of WGSI, WGSII, and WGSII mechanisms

Model	Reaction step	$E_{a,f}$ (eV)	$E_{a,b}$ (eV)	k_f (s^{-1})	k_b (s^{-1})	K_{eq}	$E_{a,obs}$ (eV)
WGSI	S1	–	–	–	–	–	–
	S2	–	–	–	–	–	–
	S3	1.93	1.54	6.07×10^{-7}	5.18×10^{-3}	1.17×10^{-4}	0.010
	S4	0.63	0.60	4.71×10^{6}	9.45×10^{6}	4.98×10^{-1}	0.045
	S5	–	–	–	–	–	–
	S6	–	–	–	–	–	–
WGSII	S1	–	–	–	–	–	–
	S2	–	–	–	–	–	–
	S3	0.72	0.92	6.20×10^{5}	5.97×10^{3}	1.04×10^{2}	0.480
	S4	1.38	0.57	2.25×10^{-1}	3.29×10^{7}	6.85×10^{-9}	− 0.415
	S5	0.63	0.60	4.71×10^{6}	9.45×10^{6}	4.98×10^{-1}	0.215
	S6	–	–	–	–	–	–
	S7	–	–	–	–	–	–
WGSIII	1	–	–	–	–	–	–
	2	0.54	0.71	6.20×10^{5}	7.81×10^{5}	7.93×10^{-1}	0.540
	3	0.83	0.96	4.62×10^{4}	2.26×10^{3}	2.04×10^{1}	0.775
	4	1.42	0.54	6.79×10^{-2}	5.04×10^{7}	1.35×10^{-9}	0.515
	5	–	–	–	–	–	–
	6	–	–	–	–	–	–

shown in Table 3, the calculated barrier of H_2O dissociation to OH and H adsorbed species (0.72 eV) for WGSII mechanism is similar to the experimental value reported by Benndorf et al. [29] and theoretical results reported by Mohsenzadeh et al. [11, 20] for HO–H bond breakage on the clean Ni surface. In the fourth step of WGSII mechanism, the adsorbed CO species reacts with the surface OH species to form COOH on the surface, which is bonded to the surface via its carbon atom (Fig.1). The calculated activation energies for this step is 1.38 eV, on the Ni (111) surface. In the fifth step of WGSII mechanism, the formate intermediate (COOHs, Table 3) subsequently dissociates to adsorbed carbon dioxide and adsorbed hydrogen with activation energies of 0.63 eV.

In the direct pathway, WGSII mechanism in Table 3, the adsorbed H_2O dissociated to OH and H adsorbed species. In the third elementary reaction in WGSII mechanism, the adsorbed OH species dissociated to OH, and H adsorbed species and in the fourth step, the adsorbed CO species interacts with the adsorbed O atoms to form adsorbed CO_2 molecules. This step is considered as the key elementary step in the CO oxidation reaction [3, 7, 11]. The activation energy obtained for this step is 1.35 eV, on the Ni (111) surface.

As shown in Table 3, the final elementary step of the WGSI, WGSII, and WGSII mechanisms is the formation of desorbed H_2 molecule. As shown in Table 3, the desorbed gas phase H_2 molecule is formed from the adsorbed H atoms. This step is endothermic and the calculated activation energies are 0.84 eV, on the Ni (111) surface.

Figures 2, 3, and 4 show the reaction profiles for the WGS reaction on Ni (111) via WGS I (Fig. 3), WGS II

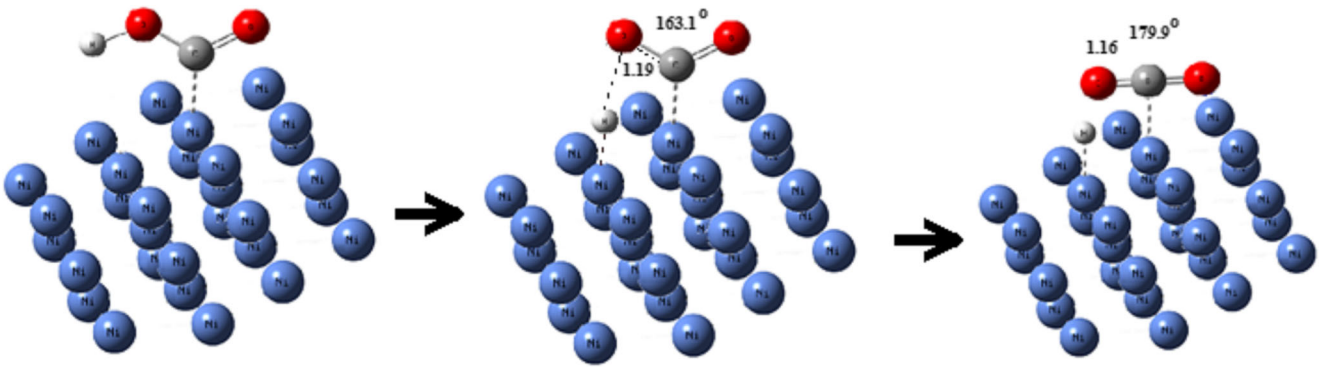

Fig. 2 The detailed configurations of initial, transition, and final states involved in WGS I (S_4 reaction step) and WGS II (S_4 reaction step) mechanisms

(Fig. 4), and WGS III (Fig. 5) mechanisms. The zero-energy reference is adsorbed water and carbon monoxide on the nickel surface. The forward and reverse barriers for each step are calculated using activation energies for the forward and reverse reactions listed in Table 3. As shown in Fig. 3, the S3 reaction step is the rate-determining step in WGS I mechanism with barrier energy about 1.93 eV, which buildup of COOH species on the surface. For WGS II mechanism in Fig. 4, it is difficult to determine the dominant pathway or the rate-determining step. In WGS II reaction profile (Fig. 4), a barrier of 1.18 eV for S3 and 1.24 eV for S4 reactions in comparison with adsorbed water and carbon monoxide is shown. In addition, for WGS III reaction profile (Fig. 5), a barrier of 0.54 eV for S2, 0.66 eV for S3, and 1.12 eV for S4 reactions in comparison with adsorbed water and carbon monoxide are shown. Thus, the S4 reaction can be considered as the rate-determining step for WGS III mechanism. By comparing of the reaction pathways in WGSI, WGS II, and WGS III mechanisms, (in Figs. 3, 4, and 5), at first glance, it can be concluded that the direct pathway is preferred on Ni (111) surface. Similar results are obtained by Mohsenzadeh et al. [11]. However, this is an inaccurate conclusion and does not match with experimental results [9]. To determine the exact preferred mechanism, it needs to take into account the effects of adsorption on the surface of the reactants. This method is done in the next section.

The forward and reverse reaction rate constants and equilibrium constants for the elementary reactions of the WGS I, WGS II, and WGS II mechanisms are calculated using Eqs. (3) and (4) and listed in Table 3. Having calculated the forward and reverse reaction rate constants and equilibrium constants for important elementary reactions involved in WGS reaction, the dominant reaction pathways for WGS reaction on Ni (111) surface are proposed.

Kinetic evaluation of different mechanisms

The kinetic surface reactions are evaluated based on the Langmuir–Hinshelwood–Hougen–Watson (LHHW) model [10, 30, 31]. In the LHHW model, it is assumed that the surface concentration of the intermediates that take part in the rate-determining reaction is much higher than that of the other intermediates [10]. In the proposed kinetic WGS I model, presented in Table 3, the reaction between adsorbed H_2O and CO species considered as the rate-determining step. Therefore, the reaction rate (R) was calculated according to this elementary step as following:

$$R = k_3\theta_{CO}\theta_{H2O} \tag{6}$$

which θ_{CO} and θ_{H2O} are surfaces occupied by CO and H_2O species and k is rate constant. The rate constant of the elementary reaction is related to activation energy (E_a) according to the Arrhenius-type equation:

$$k = A\exp\left(\frac{-E_a}{RT}\right) \tag{7}$$

where A is pre-exponential Arrhenius factor. Based on the Langmuir adsorption model, the surface occupied by CO and H_2O species are as follows:

$$\theta_{CO} = \frac{K_1P_{CO}}{1 + K_1P_{CO} + K_2P_{H_2O}} \quad \theta_{H_2O} = \frac{K_2P_{H_2O}}{1 + K_2P_{H_2O}K_1P_{CO}} \tag{8}$$

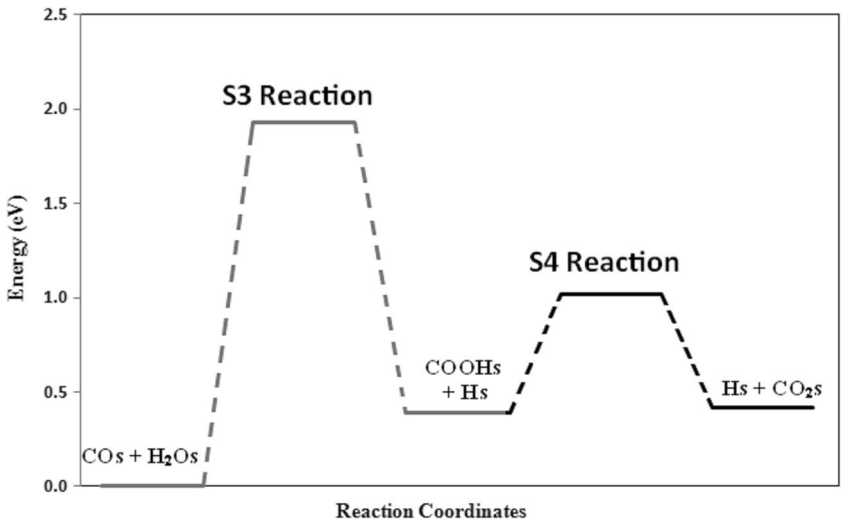

Fig. 3 The energy profiles for the WGS I mechanism pathways of WGS reaction on the Ni (111) surface

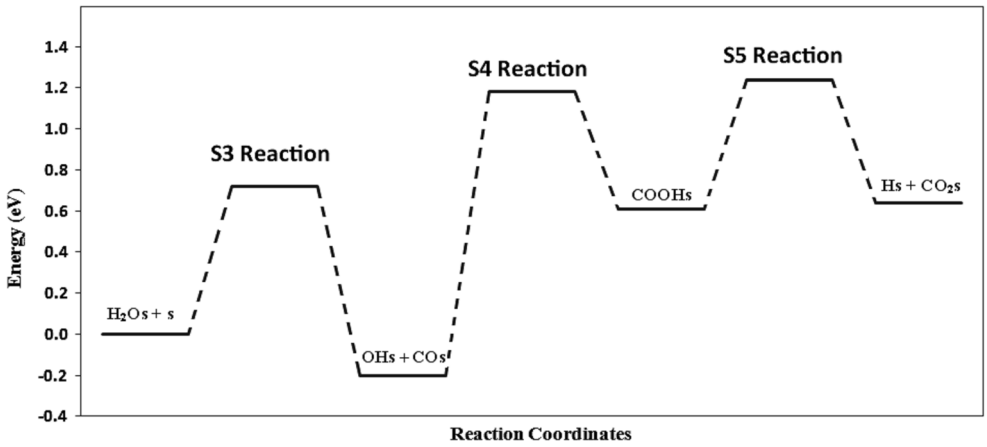

Fig. 4 The energy profiles for the WGS II mechanism pathways of WGS reaction on the Ni (111) surface

where K_1 and K_2 are adsorption constants and P_{CO} and P_{H2O} are pressures of CO and H_2O species. The H_2O and CO adsorption constants are related to the adsorption energies (E_{ads}) of these species, according to the Van't Hoff equation:

$$K_i = K_{i0}\exp\left(\frac{-E_{adsi}}{RT}\right) \tag{9}$$

Thus, by consideration of surface occupied [Eq. (6)], the WGS reaction can be changed as follows:

$$R = \frac{k_3 K_1 K_2 P_{CO} P_{H_2O}}{\left(1 + K_1 p_{CO} + K_2 P_{H_2O}\right)^2} \tag{10}$$

On the empty surface of the catalyst, K_1P_{CO} K_2P_{H2O} is lower than 1, and Eq. (10) is reduced to follow:

$$R = k_3 K_1 K_2 P_{CO} P_{H_2O} \tag{11}$$

As shown in Eq. (11), the k_{obs}, which is the apparent rate constant of the elementary reaction between adsorbed H_2O and CO, can be revealed as follows:

$$k_{obs} = k_3 K_1 K_2 \tag{12}$$

Considering Eqs. (7) and (9) in Eq. (12), the k_{obs} is changed to follow:

$$k_{obs} = A K_{1,0} K_{2,0} \exp\left[\frac{\left(-E_{a,3} - E_{ads,H_2O} - E_{ads,CO}\right)}{RT}\right] \tag{13}$$

Thus, the observed reaction energy ($E_{a,obs}$) can be revealed as follows:

$$E_{a,obs,WGS} = E_{a,3} + E_{ads,H_2O} + E_{ads,CO} \tag{14}$$

In Eq. (14), the effect of CO and H_2O adsorption energies on the activation energy of the rate-determining reaction between adsorbed H_2O and CO species is considered, which is confirmed by Sabatier principle [19]. In WGSI mechanism for rate-determined elementary reaction (4) (Table 3), the adsorbed COOH species (COOHs) converted to adsorb CO_2 species (CO_2s), the reaction rate can be written as follows:

$$R = k_4\,[S]\,[COOHs] \tag{15}$$

in which [S] is the concentration of the free active sites on the surface of the catalyst and [COOHs] is the surface concentration of the adsorbed COOH species. The concentration of the surface intermediate species such as [Hs], [COOHs], [CO_2s],

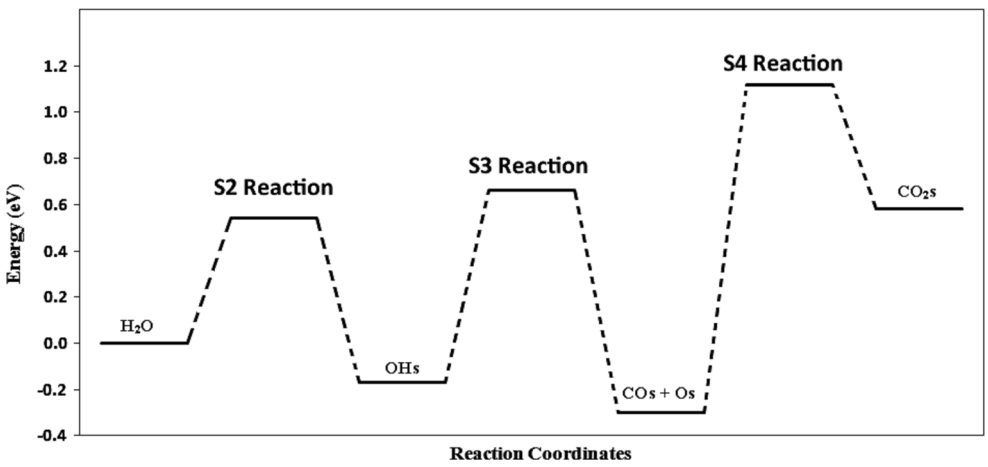

Fig. 5 The energy profiles for the WGS III mechanism pathways of WGS reaction on the Ni (111) surface

[H_2Os], and [S] must be determined for rate equations by applying quasi-equilibrium condition for elementary reactions. The quasi-equilibrium condition for elementary reaction (3), (Table 3), is shown as follows:

$$[COOHs] = \frac{K_3[COs][H_2Os]}{[Hs]} \tag{16}$$

By applying quasi-equilibrium condition for other elementary reactions, the surface [COOHs] species is related to the partial pressure of CO, H_2, and H_2O, as follows:

$$[COOHs] = K_3K_1K_2K_6^{1/2}[S]^2\frac{P_{CO}P_{H_2O}}{P_{H_2}^{1/2}} \tag{17}$$

The only remained species, [S], can be determined through balances between active and void active sites. Therefore, it is assumed that the sum of adsorbed species on the surface and void spaces are constant:

$$\theta_T = \theta s + \theta_{COOHs} \tag{18}$$

where θ_T is the total active sites on the catalyst surface, and θ_s are void sites and other active sites belonging to the adsorbed species. By substituting with $[S] = \theta s/\theta_T$ in the above equation [Eq. (18)], the following simpler equation achieved that the sum of all existing species on the surface is equal to one:

$$[\mathrm{S}] + [\mathrm{COOHs}] = 1 \tag{19}$$

For simplification assumed that surface is empty and [S] = 1. Thus, by placing Eq. (19) in Eq. (17), the reaction rate is obtained as follows:

$$R = k_4K_3K_1K_2K_6^{1/2}\frac{P_{CO}P_{H_2O}}{P_{H_2}^{1/2}} \tag{20}$$

As shown in Eq. (20), the k_{obs}, which is the apparent rate constant of the elementary reaction between adsorbed H_2O and CO, can be revealed as follows:

$$k_{obs} = k_4K_3K_1K_2K_6^{1/2} \tag{21}$$

By using the Arrhenius and Van't Hoff equations [Eqs. (7) and (9)] for thermodynamic and kinetic constants, the observed reaction energy ($E_{a,obs}$) can be revealed as follows:

$$E_{a,obs,WGS} = E_{a,4} + E_{ads,H_2O} + E_{ads,CO} + \frac{1}{2}E_{ads,H_2} + E_{a,3} \tag{22}$$

In the proposed kinetic WGS II model (Table 3), the reaction rates (R) for 3, 4, and 5 elementary reactions were calculated according to this elementary step as follows:

$$R = k_3[H_2Os][s] \tag{23}$$

$$R = k_4[COs][OHs] \tag{24}$$

$$R = k_5[COOHs][s] \tag{25}$$

Using the previous scenario for the development of reaction rates, the overall reaction rates for these elementary reactions are obtained as follows:

$$R = k_3K_2P_{H_2O} \tag{26}$$

$$R = k_4K_3K_1K_2K_7^{1/2}\frac{P_{CO}P_{H_2O}}{P_{H_2}^{1/2}} \tag{27}$$

$$R = k_5K_4K_3K_1K_2K_7^{1/2}\frac{P_{CO}P_{H_2O}}{P_{H_2}^{1/2}} \tag{28}$$

Using the same conclusion, the observed reaction energy ($E_{a,obs}$) for the previous overall reaction rates can be revealed as follows:

$$E_{a,obs} = E_{a,3} + E_{ads,H^2O} \tag{29}$$

$$E_{a,obs} = E_{a,4} + E_{a,3} + E_{ads,H^2O} + E_{ads,CO} + \frac{1}{2}E_{ads,H_2} \tag{30}$$

$$E_{a,obs} = E_{a,5} + E_{a,4} + E_{a,3} + E_{ads,H^2O} + E_{ads,CO} + \frac{1}{2}E_{ads,H_2} \tag{31}$$

The calculated activation energies for WGS reaction steps based on the developed equations [Eqs. (29–31)] for the WGSI model are shown in Table 3.

In the proposed kinetic WGS II model (Table 3), the reaction rates (R) for 3, 4, and 5 elementary reactions were calculated according to this elementary step as follows:

$$R = k_3[H_2Os][s] \tag{32}$$

$$R = k_4[COs][OHs] \tag{33}$$

$$R = k_5[COOHs][s] \tag{34}$$

Using the previous scenario for the development of reaction rates, the overall reaction rates for these elementary reactions are obtained as follows:

$$R = k_3K_2P_{H_2O} \tag{35}$$

$$R = k_4K_3K_1K_2K_7^{1/2}\frac{P_{CO}P_{H_2O}}{P_{H_2}^{1/2}} \tag{36}$$

$$R = k_5K_4K_3K_1K_2K_7^{1/2}\frac{P_{CO}P_{H_2O}}{P_{H_2}^{1/2}} \tag{37}$$

Using the same conclusion, the observed reaction energy ($E_{a,obs}$) for previous overall reaction rates can be revealed as follows:

$$E_{a,obs} = E_{a,3} + E_{ads,H^2O} \tag{38}$$

$$E_{a,obs} = E_{a,4} + E_{a,3} + E_{ads,H^2O} + E_{ads,CO} + \frac{1}{2}E_{ads,H_2} \quad (39)$$

$$E_{a,obs} = E_{a,5} + E_{a,4} + E_{a,3} + E_{ads,H^2O} + E_{ads,CO} + \frac{1}{2}E_{ads,H_2} \quad (40)$$

The calculated activation energies for WGS reaction steps, based on developed equations [Eqs. (38–40)] for WGSII model, are shown in Table 3.

In the proposed kinetic WGS III model (Table 3), the reaction rates (R) for 3, 4, and 5 elementary reactions were calculated according to this elementary step as follows:

$$R = k_2 P_{H2O} \quad (41)$$

$$R = k_3[OHs][S] \quad (42)$$

$$R = k_4[COs][Os] \quad (43)$$

Using the previous scenario for the development of reaction rates, the overall reaction rates for these elementary reactions are obtained as follows:

$$R = k_3 K_2 K_6^{1/2} \frac{P_{H_2O}}{P_{H_2}^{1/2}} \quad (44)$$

$$R = k_4 K_3 K_1 K_2 K_6 \frac{P_{CO} P_{H_2O}}{P_{H_2}} \quad (45)$$

Using the same conclusion, the observed reaction energy ($E_{a,obs}$) for the previous overall reaction rates can be revealed as follows:

$$E_{a,obs} = E_{a,2} \quad (46)$$

$$E_{a,obs} = E_{a,3} + E_{a,2} + \frac{1}{2}E_{ads,H_2} \quad (47)$$

$$E_{a,obs} = E_{a,4} + E_{a,3} + E_{a,2} + E_{ads,CO} + E_{ads,H_2} \quad (48)$$

The calculated activation energies for the WGS reaction steps based on the developed equations [Eqs. (46–48)] for WGSII model are shown in Table 3. These results are calculated based on the Sabatier principle, which takes into account the effect of adsorption on the chemical reaction [19]. Based on this principle, the optimal catalyst surface will be the trade-off between binding the reagents to the surface and not binding any of the reaction intermediates too strong relative to the product [19].

As shown in Table 3, in the WGS III mechanism, carbon dioxide is produced directly from the reaction between the adsorbed CO and O species via the direct pathway, where the overall activation energy is 0.515 eV [calculated using Eq. (48)]. In this mechanism, an overall barrier of 0.775 eV for producing Os and Hs species from adsorbed OHs is calculated using Eq. (47), and this intermediate is produced from dissociative adsorption of water with an overall barrier of 0.540 eV. In comparing with the other mechanism, direct oxidation mechanism has a larger energy barrier for all reaction steps, which causes the reaction via this mechanism to be very slow.

In the WGSII mechanism, the dissociative adsorption of water with the overall barrier of 0.480 eV [Eq. (38)] followed by the interaction between the adsorbed COs and OHs species with the overall barrier of − 0.415 eV [Eq. (39)] to produced adsorbed COOHs. Then, the adsorbed COOHs is changed to adsorbed CO_2 and Hs species, with the overall barrier of 0.215 eV [Eq. (40)]. Without considering the overall activation energies ($E_{a,obs,}$ Table 3), these two mechanisms show almost similar results based on real activation energy results (E_a, Table 3). The true behavior of the surface reaction is predictable with respect to the overall barrier of activation energies.

In the WGSI mechanism, the surface COOHs species are produced from the reaction between adsorbed COs and H_2Os with an overall barrier of 0.010 eV, which is calculated by Eq. (14). Then, these produced adsorbed COOHs species are changed to adsorbed CO_2 and Hs species, with an overall barrier of 0.045 eV, which is calculated using Eq. (22). As shown in Table 3, the elementary reaction step 4 in WGSI is the same of the elementary reaction step 5 in WGSII, but the overall activation energies of these two steps is deferent. This difference is due to the different elementary reaction steps in these two mechanisms. Thus, the WGSI mechanism provides a different path for water gas shift reaction. This different pathway involves the reaction between the adsorbed H_2O and CO species, which provides better conditions for the overall WGS reaction. The kinetic model that is developed by using the WGS I mechanism shows a better match with the experimental results in the previous works [8, 9, 13]. These results indicate that the dissociation of water on the surface of nickel is not a necessary stage in the formation of formate species.

Conclusions

The detailed mechanism and the rate of the WGS reaction on the Ni (111) surface have been studied using DFT calculation. Three sets of elementary reactions base on the formate intermediate (WGS I, WGS II) and direct oxidation mechanism (WGS III) for the WGS reaction are considered. The effect of dissociation and non-dissociation adsorption of H_2O in formate intermediate production is considered in WGSI and WGSII models. The adsorption energy for all surface species involved in these WGS reaction mechanisms was calculated. In addition, the activation barriers for the rate determining elementary steps in these mechanisms are calculated. Based on Sabatier principle, the effects of CO and H_2O adsorption energies on the activation energy of the rate-determining

reactions in the proposed mechanisms are considered. Thus, the overall activation energies are calculated using the developed kinetic models.

Based on the calculated overall activation energies, the formate intermediates show the best reaction route in the WGS surface mechanism. The results show that the mechanism WGSI that provides a different path for the production of formate intermediates is the best model in our proposed WGS reaction models. This different pathway involves the reaction between adsorbed H_2O and CO species, which provides better conditions for the overall WGS reaction.

Funding information Financial support was provided by the Ferdowsi University of Mashhad, Iran (Grant No. 2 /45992-11/7/96).

Compliance with ethical standards

Conflict of interest The authors declare that they have no conflict of interest.

References

1. LeValley TL, Richard AR, Fan M (2014) The progress in water gas shift and steam reforming hydrogen production technologies—a review. Int J Hydrog Energy 39(30):16983–17000
2. Lang C, Sécordel X, Courson C (2017) Copper-based water gas shift catalysts for hydrogen rich syngas production from biomass steam gasification. Energy Fuel 31(11):12932–12941
3. Wheeler C, Jhalani A, Klein E, Tummala S, Schmidt L (2004) The water–gas-shift reaction at short contact times. J Catal 223(1):191–199
4. Catapan RC, Oliveira AA, Chen Y, Vlachos DG (2012) DFT study of the water–gas shift reaction and coke formation on Ni (111) and Ni (211) surfaces. J Phys Chem C 116(38):20281–20291
5. Sanchez-Escribano V, Vargas ML, Finocchio E, Busca G (2007) On the mechanisms and the selectivity determining steps in syngas conversion over supported metal catalysts: an IR study. Appl Catal A Gen 316(1):68–74
6. Seok S-H, Han SH, Lee JS (2001) The role of MnO in Ni/MnO-Al 2 O 3 catalysts for carbon dioxide reforming of methane. Appl Catal A Gen 215(1):31–38
7. Smith R, Loganathan M, Shantha MS (2010) A review of the water gas shift reaction kinetics. Int J Chem React Eng 8(8):4
8. Nakhaei Pour A, Housaindokht MR, Tayyari SF, Zarkesh J, Shahri SMK (2011) Water-gas-shift kinetics over a Fe/cu/La/Si catalyst in Fischer–Tropsch synthesis. Chem Eng Res Des 89(3):262–269
9. Nakhaei Pour A, Housaindokht MR, Zarkesh J, Tayyari SF (2010) Water-gas-shift kinetic over nano-structured iron catalyst in Fischer–Tropsch synthesis. J Nat Gas Sci Eng 2(2):79–85
10. Van Der Laan GP, Beenackers A (1999) Kinetics and selectivity of the Fischer–Tropsch synthesis: a literature review. Cat Rev Sci Eng 41(3–4):255–318
11. Mohsenzadeh A, Richards T, Bolton K (2016) DFT study of the water gas shift reaction on Ni (111), Ni (100) and Ni (110) surfaces. Surf Sci 644:53–63
12. Lin C-H, Chen C-L, Wang J-H (2011) Mechanistic studies of water–gas-shift reaction on transition metals. J Phys Chem C 115(38): 18582–18588
13. Nakhaei Pour A, Housaindokht M, Torabi F (2014) Water–gas shift kinetics over lanthanum-promoted iron catalyst in Fischer–Tropsch synthesis: thermodynamic analysis of nanoparticle size effect. J Iran Chem Soc 11(6):1639–1648. https://doi.org/10.1007/s13738-014-0435-5
14. Cerda JR, Andres PL, Cebollada A, Miranda R, Navas E, Schuster P, Schneider CM, Kirschner J (1993) Epitaxial growth of cobalt films on Cu(100): a crystallographic LEED determination. J Phys Condens Matter 5(14):2055
15. Giannozzi P, Baroni S, Bonini N, Calandra M, Car R, Cavazzoni C, Ceresoli D, Chiarotti GL, Cococcioni M, Dabo I (2009) QUANTUM ESPRESSO: a modular and open-source software project for quantum simulations of materials. J Phys Condens Matter 21(39):395502
16. Nakhaei Pour A, Keyvanloo Z, Izadyar M, Modaresi SM (2015) Dissociative hydrogen adsorption on the cubic cobalt surfaces: a DFT study. Int J Hydrog Energy 40(22):7064–7071
17. Nakhaei Pour A, Karimi J, Keyvanloo Z, Hashemian M (2016) Size dependence adsorption of hydrogen on cobalt clusters: a DFT study. In: Journal of Nano Res. Trans Tech Publ, pp 100–111
18. Jeon YT, Moon JY, Lee GH, Park J, Chang Y (2006) Comparison of the magnetic properties of metastable hexagonal close-packed Ni nanoparticles with those of the stable face-centered cubic Ni nanoparticles. J Phys Chem B 110(3):1187–1191
19. Niemantsverdriet J (2006) Concepts of modern catalysis and kinetics. John Wiley & Sons, Hoboken
20. Mohsenzadeh A, Bolton K, Richards T (2014) DFT study of the adsorption and dissociation of water on Ni (111), Ni (110) and Ni (100) surfaces. Surf Sci 627:1–10
21. Fajín JL, Cordeiro MND, Illas F, Gomes JR (2010) Descriptors controlling the catalytic activity of metallic surfaces toward water splitting. J Catal 276(1):92–100
22. Seenivasan H, Tiwari AK (2013) Water dissociation on Ni (100) and Ni (111): effect of surface temperature on reactivity. J Chem Phys 139(17):174707
23. Zhou Y-H, Lv P-H, Wang G-C (2006) DFT studies of methanol decomposition on Ni (100) surface: compared with Ni (111) surface. J Mol Catal A Chem 258(1):203–215
24. Christmann K, Behm R, Ertl G, Van Hove M, Weinberg W (1979) Chemisorption geometry of hydrogen on Ni (111): order and disorder. J Chem Phys 70(9):4168–4184
25. Ren J, Meng S (2008) First-principles study of water on copper and noble metal (110) surfaces. Phys Rev B 77(5):054110
26. Vesselli E, Rogatis LD, Ding X, Baraldi A, Savio L, Vattuone L, Rocca M, Fornasiero P, Peressi M, Baldereschi A (2008) Carbon dioxide hydrogenation on Ni (110). J Am Chem Soc 130(34): 11417–11422
27. Stuckless J, Al-Sarraf N, Wartnaby C, King D (1993) Calorimetric heats of adsorption for CO on nickel single crystal surfaces. J Chem Phys 99(3):2202–2212
28. Christmann K, Schober O, Ertl G, Neumann M (1974) Adsorption of hydrogen on nickel single crystal surfaces. J Chem Phys 60(11): 4528–4540
29. Benndorf C, Madey TE (1988) Adsorption of H2O on clean and oxygen-preposed Ni (110). Surf Sci 194(1–2):63–91
30. Nakhaei Pour A, Housaindokht MR (2017) A new kinetic model for direct CO2 hydrogenation to higher hydrocarbons on a precipitated iron catalyst: effect of catalyst particle size. J Energy Chem 26(3):359–367
31. Nakhaei Pour A, Housaindokht MR, Monhemi H (2016) A new LHHW kinetic model for CO_2 hydrogenation over an iron catalyst. Prog React Kinet Mech 41(2):159–169